

Using ERS-2 SAR images for routine observation of marine pollution in European coastal waters

Martin Gade*, Werner Alpers

Institut für Meereskunde, Universität Hamburg, D-22529 Hamburg, Germany

Abstract

More than 660 synthetic aperture radar (SAR) images acquired over the southern Baltic Sea, the North Sea, and the Gulf of Lion in the Mediterranean Sea by the Second European Remote Sensing Satellite (ERS-2) have been analyzed since December 1996 with respect to radar signatures of marine pollution and other phenomena causing similar signatures. First results of our analysis reveal that the seas are most polluted along the main shipping routes. The sizes of the detected oil spills vary between $< 0.1 \text{ km}^2$ and $> 56 \text{ km}^2$. SAR images acquired during descending (morning) and ascending (evening) satellite passes show different percentages of oil pollution, because most of this pollution occurs during night time and is still visible on the SAR images acquired in the morning time. Moreover, we found a higher amount of oil spills on SAR images acquired during summer (April–September) than on SAR images acquired during winter (October–March). We attribute this finding to the higher mean wind speed encountered in all three test areas during winter. By using an ERS-2 SAR image of the North Sea test area we show how the reduction of the normalized radar backscattering cross section (NRCS) by an oil spill depends on wind speed. © 1999 Elsevier Science B.V. All rights reserved.

Keywords: Remote sensing; Oil pollution; SAR; European coastal waters

1. Introduction

‘Clean Seas’ is a project funded by the European Community (EC), which is aimed at investi-

gating the application of satellite data for coastal management, particularly for monitoring marine (oil) pollution. Within this project, three test areas in European marginal waters, the southern Baltic Sea and North Sea, and the Gulf of Lion in the Mediterranean (see Fig. 1), were chosen to detect any marine pollution, be it, e.g. from ship operations or from river runoffs. The test areas include major ship routes, like the Strait of Born-

* Corresponding author. Tel.: +49-40-42838-5450; fax: +49-40-42838-5713.
E-mail address: gade@ifm.uni-hamburg.de (M. Gade)

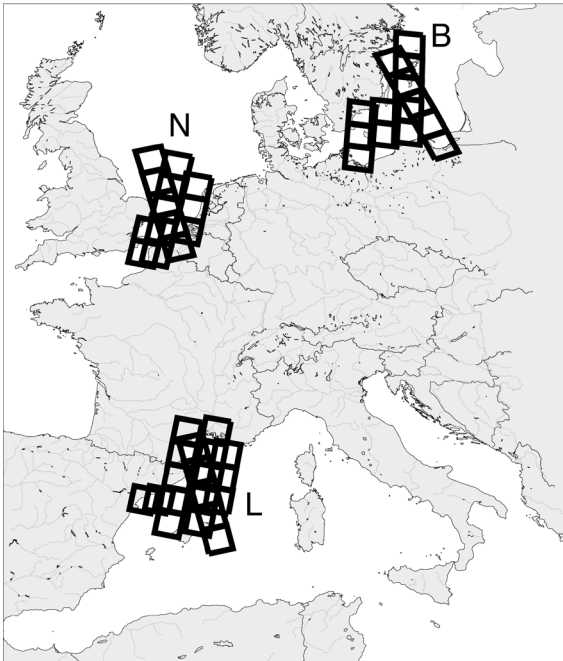


Fig. 1. Map of the three test areas (B: Baltic Sea, N: North Sea, and G: Gulf of Lion). The rectangles denote the location of the ERS-2 SAR frames which are regularly acquired and analyzed.

holm (Baltic Sea), the English Channel (North Sea), and the sea area between the harbors of Marseille and Barcelona (Mediterranean), and, moreover, the estuaries of the major rivers Oder (Baltic Sea), Thames, Rhine (North Sea), and Rhone (Mediterranean). Amongst scientists from six European countries, members of the research group Satellite Oceanography of the University of Hamburg have been participating in Clean Seas by analyzing synthetic aperture radar (SAR) images acquired from the Second European Remote Sensing Satellite (ERS-2). In addition to the ERS-2 SAR, various optical and microwave sensors, like the Advanced Very High Resolution Radiometer (AVHRR) aboard the NOAA satellites, and the Along-track Scanning Radiometer (ATSR) aboard the ERS-2 have been used for routine studies within Clean Seas. However, in this paper we concentrate on results obtained from the analysis of the ERS-2 SAR images.

For each of the three test areas 15 SAR frames were chosen for routinely monitoring marine pol-

lution (the locations of the SAR frames are depicted in Fig. 1. For the Gulf of Lion the total number of frames is higher, because two additional frames have been chosen for our analyses). Since the start of the project on December 1 1996, a total of 664 ERS-2 SAR images acquired over the three test areas (as by September 26 1998, i.e. after 19 repeat cycles of the ERS-2) have been analyzed. Oil films floating on the sea surface dampen the small-scale surface waves, and since these waves are responsible for the radar backscattering at oblique incidence angles (between 20° and 75°; so-called Bragg scattering) they are visible on SAR images as areas of reduced backscattered radar power (see, e.g. Alpers and Hühnerfuss (1988), Gade et al. (1998a), and literature cited therein). Apart from definite oil pollution (i.e. dark patches in the SAR images which can clearly be related to oil spills) the images show a large variety of radar signatures caused by oceanic and atmospheric phenomena, some of which look similar to radar signatures of oil spills and therefore are often called 'look-alikes' (Espedal et al., 1995).

In this paper, after showing some examples of oil spills and look-alikes, we briefly summarize the first results of our statistical analysis from each of the three test areas.

2. Results

In this analysis we have used ERS-2 SAR images which were processed to a resolution of 100 m. These so-called 'quick-look images' were provided by the West Freugh Ground Station in Scotland, UK. These quick-look images are advantageous because the dark signatures of oil spills can still be delineated, but the small size of the data files makes it easier to quickly process a large amount of SAR images. As a first step, we have analyzed every SAR image with respect to the occurrence of oil pollution. In order to ensure maximum confidence of the oil detection and, thus, of the statistics to be produced, this analysis was done by eye. The detected oil spills have then been (manually) catalogued by means of their exact position, size, and their mean reduction of

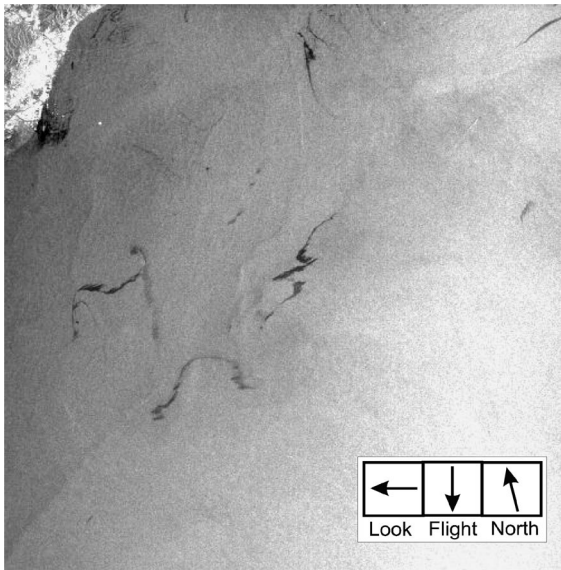


Fig. 2. ERS-2 SAR image of the Mediterranean Sea off the Spanish coast (orbit 12759, frame 2781, acquired on 28 September 1997, 10:35 UTC, image dimensions $100 \text{ km} \times 100 \text{ km}$, image center at $40^{\circ}58'N/2^{\circ}36'E$). We hypothesize that the dark irregular patches in the middle of the image are caused by marine oil pollution (oil spills).

the radar backscattering in that particular area.

Fig. 2 shows an ERS-2 SAR image acquired over the Mediterranean Sea off the Spanish coast on September 28 1997, at 10:35 UTC. On the top right corner of the image the city of Barcelona can be delineated as a bright area (high backscattered radar power). Bright spots off the coast are due to ships. We attribute the dark irregular patches in the middle of the image to marine oil pollution, because of their isolated occurrence and their elongated shape. The irregular shape of these spills is caused by the action of the wind and by the local sea current. When analyzing the acquired SAR images we often found radar signatures of oil spills on SAR images of the sea surface which cover an area larger than 10 km^2 .

In order to demonstrate the encountered difficulties in undoubtedly identifying oil pollution on SAR images of the sea surface, we show two additional SAR images (Figs. 3 and 4). Fig. 3 shows a SAR image acquired on January 5 1997, at 09:50 UTC over the Baltic Sea south of Gotland. All along the southern coast line dark

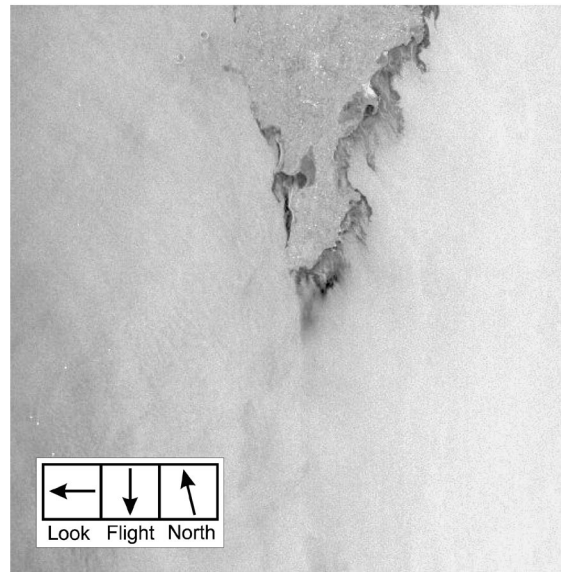


Fig. 3. ERS-2 SAR image of the Baltic Sea south of Gotland (orbit 8951, frame 2457, acquired on 5 January 1997, 09:50 UTC, image dimensions $100 \text{ km} \times 100 \text{ km}$, image center at $56^{\circ}52'N/18^{\circ}6'E$). The dark signatures south of Gotland are very likely due to grease ice.

patches are visible. These patches, however, are not caused by surface films, but by grease ice which was driven off the coast by a northerly wind (from AVHRR and ATSR imagery of that time period we inferred that the sea surface temperature (SST) along the coastline was 0°C or even less). The small-scale waves which are responsible for the radar backscattering are damped by the ice and, thus, the icy areas are visible as dark regions. Because of the meteorological conditions during the acquisition time, and since it is unlikely that oil pollution occurred all the coastline, these signatures were identified as being caused by look-alikes.

In Fig. 4, a SAR image is shown which was acquired on June 12 1997, at 10:29 UTC over the Gulf of Lion. Various dark features of different shape are visible on this image. For example, the elongated dark features in the upper image half are typical for being caused by natural sea slicks (in contrast to the isolated dark radar signatures in Fig. 1), whereas the small-scale regular black patches in the middle of the image are due to atmospheric convective cells. The radially blowing

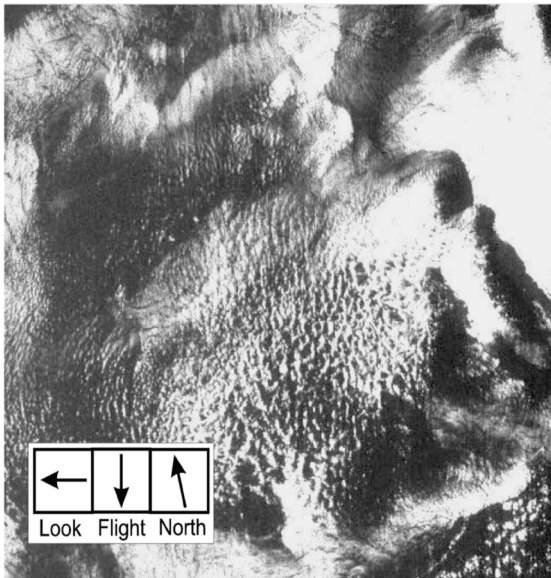


Fig. 4. ERS-2 SAR image of the Gulf of Lion (orbit 11213, frame 2745, acquired on 12 June 1997, 10:29 UTC, image dimensions $100 \text{ km} \times 100 \text{ km}$, image center at $42^{\circ}44'N/4^{\circ}31'E$). We attribute the various dark signatures to be due to different oceanic and atmospheric phenomena.

wind within these cells causes enhancement or reduction of the radar backscattering, depending on, for example, the direction of the underlying wind field and the SAR look direction. None of the features visible in Fig. 4, however, can clearly be related to marine oil pollution.

During the first 19 repeat cycles of the ERS-2 within Clean Seas, a total of 200 SAR images have been acquired over the Baltic Sea test area (some images were acquired only during every second overpass). Fig. 5 shows the location of all detected oil spills in the Baltic Sea test area between December 1 1996, and September 26 1998. Typical criteria for the classification of the radar signatures as being caused by oil pollution were isolated occurrence, elongated shape, and sharp edges. The left map shows the location and sizes of all spills which were detected on ERS SAR images acquired between April and September (either 1997 or 1998). The right map shows the corresponding oil spill sizes and locations detected on ERS SAR images acquired between October and March (since December 1996). In

both maps the sizes of the circles are proportional to the sizes of the oil spills. It is obvious that the oil spills follow the main shipping routes (passing north of the island of Bornholm and east of Gotland). Only a few oil spills are observed off these routes. Moreover, the maps clearly show that in the winter season there are fewer radar signatures of oil pollution (right map of Fig. 5).

Fig. 6 shows a bar chart of the number of ERS SAR images acquired during each repeat cycle over the Gulf of Lion test area since the beginning of the project. For each cycle the dark (bottom) bars denotes the number of SAR images showing oil spills, and the bright (top) bars denotes the amount of SAR images without oil pollution. The total number of SAR images which have been recorded during a cycle (lasting 35 days) varies because some SAR images have been acquired only during every second overpass. In addition to the bars we have included a curve denoting the percentages of SAR frames showing oil pollution (see the scale on the right-hand side of Fig. 6). Although the effect of the annual variation of the oil pollution is less pronounced in the Gulf of Lion than in the Baltic Sea test area, we also find maximum percentages of oil pollution during the summer months (see the maxima of the curve at late September 1997 and early July 1998).

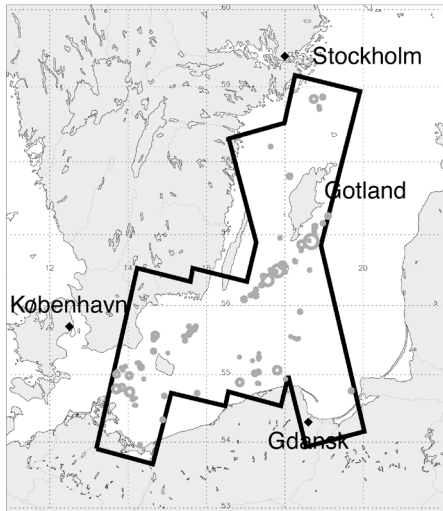
For each frame (see Fig. 1) the percentage of SAR images showing marine oil pollution has been determined and is shown in Fig. 7. Dark-colored frames denote high occurrences of oil pollution in the respective area, and bright frames denote low pollution. We found the highest occurrence of oil pollution south of Barcelona, off the Spanish coast (see the dark frames in Fig. 7). Moreover, it can be seen that, on average, the descending (morning) passes (reaching from north-east to south-west) show higher occurrence of oil spills than the ascending (evening) passes (reaching from south-east to north-west).

3. Discussion

It is noteworthy that the detectability of oceanic surface films by SAR sensors strongly depends on

Spill Sizes

Range: 0.1 - 36.9 km
 Period: Apr. 1997 - Aug 1998
 Legend: ● = 1 km ○ = 10 km ○ = 25 km ○ = 50 km



Range: 0.1 - 14.8 km
 Period: Dec. 1996 - Mar 1998
 Legend: ● = 1 km ○ = 10 km ○ = 25 km ○ = 50 km

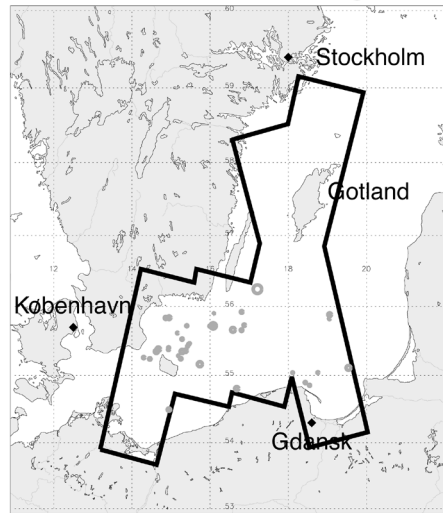


Fig. 5. Locations of the detected oil pollution within the Baltic Sea test area. The size of the circles are proportional to the size of the detected oil spills. The polygon denotes the area coverage by the ERS-2 SAR frames. Left map: spills detected during summer (April–September), right map: spills detected during winter (October–March). The polygons added into each map denote the total coverage of the SAR frames (see Fig. 1).

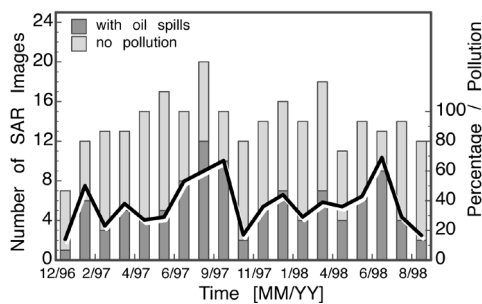


Fig. 6. Bar chart of the number of ERS SAR images of the Gulf of Lion test area used in this investigation showing radar signatures of oil pollution and no oil (left-hand scale). The black curve denotes the time series of the percentage of ERS SAR frames showing oil spills in the Gulf of Lion test site (right-hand scale).

wind speed: at either very low wind speeds (below approx. 2 m/s) or very high wind speeds (above approx. 10 m/s) oceanic surface films cannot (or only barely) be identified. In order to show this strong wind speed dependence, we have analyzed a SAR image acquired over the North Sea test

area on March 14 1997, at 10:40 UTC (Fig. 8). At the time of the image acquisition, an atmospheric front passed the area, so that the wind speed strongly increased (which in turn results in different intensities of the radar backscatter on both sides of the front, see Fig. 8a). South-west of the front, surface films are visible as dark patches and lines, whereas north-east of the front no such signatures can be observed. A dark patch corresponding to a surface film is placed exactly on the front line (see the enlarged part of the SAR image shown in Fig. 8b). In order to study the dependence of the radar signature of a surface film on wind speed we have calculated the reduction of the normalized radar backscattering cross section (NRCS) along the scan line inserted into Fig. 8b. From this scan (see Fig. 8c) we see that on the low-wind side (towards point A), the NRCS reduction is about 10 dB (i.e. the NRCS drops down to the noise floor), whereas it is only about 6 dB on the high-wind side (towards point B, see the horizontal lines added into the scan). This

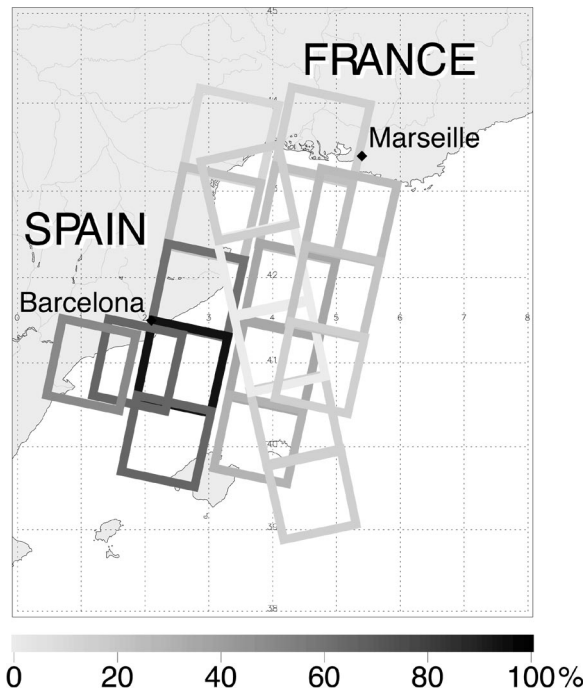


Fig. 7. Map of the percentages of ERS SAR images acquired between 1 December 1996, and 26 September 1998, over the Gulf of Lion test area and showing mineral oil spills. Note that during the ascending (evening) passes (that is, the passes going from south-east to north-west) less oil pollution has been detected.

finding is in accordance with recently presented results of field experiments in the North Sea

(Gade et al., 1998b): the reduction of the NRCS by marine surface films decreases with increasing wind speed, because at high wind speeds, wave breaking and the permanent action by the wind cause a reduced overall damping capability of the surface film. On the right-hand side of the panel in Fig. 8c the wind speed is added which has been calculated from the NRCS values by using a wind scatterometer model for retrieving sea surface winds from ERS scatterometer data [the so-called CMOD-4 model (Stoffelen and Anderson, 1997)]. It is well visible that with increasing wind speed the surface roughness and, thus, the backscattered radar power increases. This wind scatterometer model seems to underestimate the wind speed in the slick-free areas of the water surface, since a minimum wind speed of approximately 2 m/s is needed for the generation of the small-scale surface roughness which is responsible for the radar backscattering. However, it is obvious that an additional underestimation of the wind speed is caused when the water surface is slick-covered, because of the additional reduction of the NRCS by the slick.

Table 1 summarizes the results presented in the last chapter more quantitatively. The upper section (upper two rows) shows the total number of analyzed SAR frames as well as the total spill-covered area per test area (Baltic Sea, North Sea, and Gulf of Lion). From these data we can

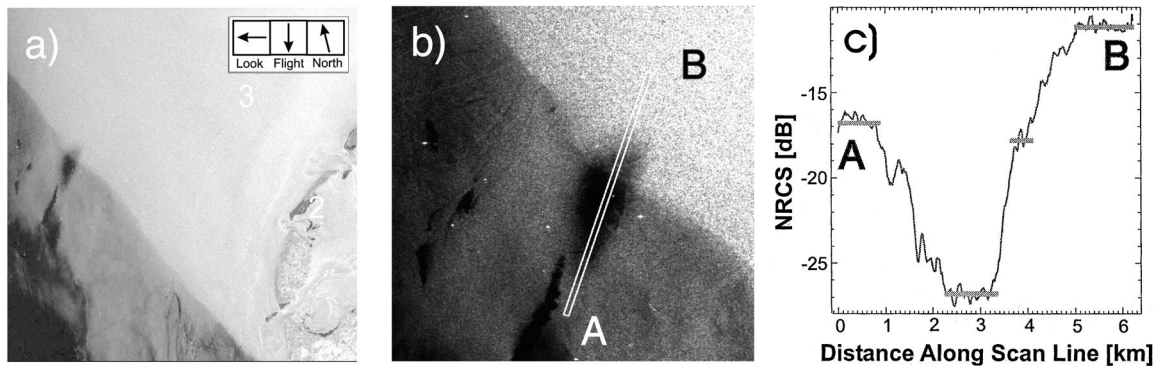


Fig. 8. (a) ERS-2 SAR image of the North Sea west of the West Frisian Islands (orbit 10068, frame 2529, acquired on 24 March 1997, 10:40 UTC, image dimensions 100 km \times 100 km, image center at 53°21'N/4°26'E) showing radar signatures of oil pollution and of an atmospheric front; (b) section (25 km \times 25 km) of the SAR image showing a surface slick shown in a); (c) image intensity scan along the line shown in (b). The right scale denotes the wind speed derived from the normalized radar backscattering cross section (NRCS).

Table 1
Results from the analyses of the ERS-2-SAR images of the three test sites

Test area	Baltic Sea	North Sea	Gulf of Lion
Total number of SAR images	200	196	268
Total spill-covered area (km ²)	522.2	721.8	1059.6
<i>Percentage of scenes with...</i>			
(a) Spill(s)	26	31	38
Small spill(s) (1 km ²)	16	17	21
Large spill(s) (1 km ² –5 km ²)	18	21	23
Very large spill(s) (> 5 km ²)	9	11	17
<i>Total number of...</i>			
Spills	179	194	302
Small spills (≤ 1 km ²)	73	70	101
Large spills (1 km ² –5 km ²)	77	90	142
Very large slicks (> 5 km ²)	29	34	59
<i>Total number of spills in...</i>			
All scenes	142/37	127/67	213/89
Descending scenes (am), summer/winter	106/30	104/59	213/86
Ascending scenes (pm), summer/winter	36/7	23/8	0/3

delineate that the spill-coverage per SAR image is lowest in the Baltic Sea (2.61 km²) and highest in the Gulf of Lion (3.95 km²).

In the second section of Table 1 the percentage of SAR images showing oil pollution is shown. It can be seen that we have detected the highest percentage of oil pollution in the Gulf of Lion test area (38% of the images, see the right-most column) and that about 20% of all images show radar signatures of large oil spills with sizes ranging from 1 km² to 5 km². In the Gulf of Lion the relative number of very large oil spills (> 5 km²) is higher than in the other two areas. This we attribute to the fact that the test site includes the sea area off Barcelona which is an area of high spatial density of oil pollution (e.g. in front of the harbor of Barcelona we often observed a large plume driven by the coastal current towards south).

The third section of Table 1 shows the total number of oil spills detected in the SAR images from all test areas. It can be seen that the highest occurrence of oil spills is found in the Gulf of Lion test area. Even spills with a size > 1 km² have are found in the Gulf of Lion more often than in the North Sea and Baltic Sea.

The bottom section of Table 1 shows the distribution of the detected oil spills on the different overpasses (that is, descending (morning) and ascending (evening)) as well as on the different seasons (summer and winter). In all three test areas the occurrence of oil pollution detected on SAR images acquired during descending passes is much higher than during ascending passes. We attribute this finding to the fact that oil is spilled from ships most frequently during night time. Since the oil spills may stay on the water surface for some hours (or even more, depending on kind and amount of the slick material, sea state, and wind conditions) they are still visible on SAR images acquired during morning passes. This observed difference is most pronounced during summer months and less pronounced during the winter months, because of the earlier sunset (the evening passes are between 21:00 and 22:00 UTC). Moreover, the finding that more pollution is detected during summer months (between April and September) may be due to the fact that the mean wind speed in all three test areas is lower during summer. Thus, any oil pollution might be easier to detect because of the wind speed dependence

of the visibility of oil spills on SAR images (see Fig. 8).

4. Conclusions

More than 660 ERS-2 SAR images have been acquired since December 1996, over the three Clean Seas test areas (Baltic Sea, North Sea, and Gulf of Lion). This large number of SAR images of the ocean surface of European coastal waters has allowed for a systematic statistical analysis. Our most important findings are that (1) the systematic analysis of SAR images proves former observations made by oil-pollution control agencies or coast guards, that most pollution occurs along the main ship traffic routes, (2) the number of detected oil spills depends on season, and (3) oil spills are more often detected on SAR images acquired during descending (morning) passes than during ascending (evening) passes.

We are aware that the total amount of particular SAR images (see the rectangles inserted into Fig. 1) is not high enough to allow statistics of high confidence (the particular SAR frames have been acquired only up to 18 times). However, we believe that our findings are significant for the interpretation of the usage of satellite-borne radar techniques for the monitoring of oil pollution.

Several ERS-2 SAR images showing so-called look-alikes (that is, showing radar signatures looking similar than those caused by oil pollution) have been acquired within the Clean Seas project. Therefore, we conclude that for an effective oil spill surveillance system a good understanding is required of radar signatures caused by oceanic and atmospheric phenomena that give rise to similar radar signatures as those by oil spills. However, the long repeat cycle of the ERS-2 (35 days) and the SAR processing time (some hours) are also limiting factors for an operational oil surveillance.

Future statistical analysis of SAR images will comprise, e.g. the consideration of mean wind speed in the particular areas during image acquisition, a better classification of the observed

phenomena, particularly of the observed oil pollution, and synoptic studies using optical and microwave data from the other sensors used within the Clean Seas project. Moreover, advanced image analysis techniques, like, e.g. the calculation of the fractal dimensions of the observed signatures, shall be applied within our studies (since fractal dimensions can be used as a measure of the diffusiveness of the observed signatures, they may yield additional information on the signatures' origin which in turn may improve automated oil spill detection algorithms).

Acknowledgements

The authors are grateful to M. Keßler, S. Ufermann, D. Gruber, and J. Scholz for their engaged help in data processing and for generating the web site for the members of the Clean Seas project. Furthermore, we would like to thank G.W. Jolly from Satellite Observing Systems, UK, for the coordination of the Clean Seas project and for swiftly forwarding the SAR images. This work has been supported by the European Community under contract ENV4-CT96-0334, 'Clean Seas'.

References

- Alpers W, Hühnerfuss H. Radar signatures of oil films floating on the sea surface and the Marangoni effect. *J Geophys Res* 1988;93:3642–3648.
- Espedal HA, Johannessen OM, Knulst J. Natural films in coastal waters, *Proceed. Int. Geosci. Remote Sens. Sympos. Florence, Italy: (IGARSS)'95, 1995:2106–2108.*
- Gade M, Alpers W, Hühnerfuss H, Masuko H, Kobayashi T. Imaging of biogenic and anthropogenic ocean surface films by the multifrequency/multipolarization SIR-C/X-SAR. *J Geophys Res* 1998a;103:18851–18866.
- Gade M, Alpers W, Hühnerfuss H, Wismann VR, Lange PA. On the reduction of the radar backscatter by oceanic surface films. Helicopter measurements and their theoretical interpretation. *Remote Sens Environ* 1998b;66:52–70.
- Stoffelen A, Anderson D. Scatterometer data interpretation. Estimation and validation of the transfer function CMOD4. *J Geophys Res* 1997;102:5767–5780.